

Snow-cover mapping in forests by constrained linear spectral unmixing of MODIS data

Dagrun Vikhamar^{a,*}, Rune Solberg^b

^aDepartment of Geosciences, University of Oslo, P.O. Box 1047 Blindern, N-0316 Oslo, Norway

^bNorwegian Computing Center, P.O. Box 114 Blindern, N-0314 Oslo, Norway

Received 28 January 2003; received in revised form 18 June 2003; accepted 20 June 2003

Abstract

A snow-cover mapping method accounting for forests (*SnowFrac*) is presented. *SnowFrac* uses spectral unmixing and endmember constraints to estimate the snow-cover fraction of a pixel. The unmixing is based on a linear spectral mixture model, which includes endmembers for snow, conifer, branches of leafless deciduous trees and snow-free ground. Model input consists of a land-cover fraction map and endmember spectra. The land-cover fraction map is applied in the unmixing procedure to identify the number and types of endmembers for every pixel, but also to set constraints on the area fractions of the forest endmembers. *SnowFrac* was applied on two Terra Moderate Resolution Imaging Spectroradiometer (MODIS) images with different snow conditions covering a forested area in southern Norway. Six experiments were carried out, each with different endmember constraints. Estimated snow-cover fractions were compared with snow-cover fraction reference maps derived from two Landsat Enhanced Thematic Mapper Plus (ETM+) images acquired the same days as the MODIS images. Results are presented for non-forested areas, deciduous forests, coniferous forests and mixed deciduous/coniferous forests. The snow-cover fraction estimates are enhanced by increasing constraints introduced to the unmixing procedure. The classification accuracy shows that 96% of the pixels are classified with less than 20% error (absolute units) on 7 May 2001 when all forested and non-forested areas are included. The corresponding figure for 4 May 2000 is 88%.

© 2003 Elsevier Inc. All rights reserved.

Keywords: Remote sensing; Snow mapping; Forest; Unmixing; Spectral mixture model; MODIS

1. Introduction

Improving the techniques for global and regional snow-cover mapping may benefit both environmental interests and hydrological applications. Climate changes may influence the spatial extent of the snow (Barnett, Dümenil, Schlese, Roeckner, & Latif, 1989; Cess et al., 1991; Cohen & Entekhabi, 2001). Improved parameterization of the snow-cover extent is needed to enhance climate predictions (Roesch, Wild, Gilgen, & Ohmura, 2001). In seasonally snow-covered regions, the snow cover affects the ecology (Jones, 1999; Walker, Halfpenny, Walker, & Wessman, 1993), the vegetation pattern (Gjærevoll, 1956) and the hydrological cycle. Information about the contribution of snowmelt to the runoff is substantial for water resource management (irrigation, flood prediction, hydropower pro-

duction). Damaging floods have been caused by intensive snowmelt and rain-on-snow events (Lundquist, Lunde, & Bøe, 1996; Marks, Kimball, Tingey, & Link, 1998; Sui & Koehler, 2001). In Norway, where 99% of the electricity is produced from hydropower, 25–50% of the precipitation falls as snow (Winther & Hall, 1999; Wold, 1992). Another country where snowmelt is important for hydropower production is Switzerland, which produces 60% of the electricity from hydropower (Beniston, 1997). In these regions, the quality of the runoff forecast depends on the reliability of the snow-cover estimate.

Various techniques for surveying the snow coverage on regional and global scales exist. Meteorological observations and regular manual surveys of snow depth and snow density are traditional methods to estimate the snow water equivalent and to follow the evolution of the snow cover. Snow pillows are also used for snow monitoring (Sorteberg, Engeset, & Udnæs, 2001). Contrary to the mentioned techniques, satellite images provide continuous spatial measurements, acquired globally at regular intervals. A

* Corresponding author. Tel.: +47-2285-5927; fax: +47-2285-4215.
E-mail address: dagrun.vikhamar@geo.uio.no (D. Vikhamar).

number of methods for snow-cover mapping have been developed for optical as well as for active and passive microwave sensors (see review by König, Winther, and Isaksson, 2001). For global monitoring of the snow-covered areas, images from optical and passive microwave sensors are currently most suitable (Hall, Kelly, Riggs, Chang, & Foster, 2002; Romanov, Gutman, & Csiszar, 2000; Solberg et al., 1997). Because the spatial resolution of the satellite images from today's passive microwave sensors is coarse (5–25 km), and the active microwave sensors still do not provide reliable information about the snow, optical images are often applied in regional snow monitoring. Several snow monitoring systems using optical images for runoff forecasts have been developed (Baumgartner & Rango, 1995; Haefner, Seidel, & Ehrlert, 1997; Solberg & Andersen, 1994).

A problem for optical images, and also microwave images, occurs in forested regions. Trees mask parts of the snow-covered ground, as well as contribute to the satellite-measured radiance. To improve the mapping of snow in forests, the effects of trees should be accounted for, otherwise, the snow cover may be underestimated in forested areas, as has been observed with the Norwegian Linear Reflectance-to-Snow-Cover algorithm (Solberg et al., 1997). A few studies have particularly focused on handling the forest problem for snow-cover mapping (Klein, Hall, & Riggs, 1998; Metsämäki, Vepsäläinen, Pulliainen, & Sucksdorff, 2002). It has been demonstrated that snow in forests is mapped with lower precision than in non-forested areas using the Moderate Resolution Imaging Spectroradiometer (MODIS) snow mapping algorithm (Hall, Foster, Salomonson, Klein, & Chien, 2001) and a linear interpolation method (Metsämäki et al., 2002). Another promising approach for estimating subpixel snow cover is spectral unmixing (Nolin, Dozin, & Mertes, 1993; Painter, Roberts, Green, & Dozier, 1998; Rosenthal & Dozier, 1996). These spectral unmixing studies have included snow-covered mountains and some forested areas, but have not specifically investigated different forest types (tree species, densities).

The objective of study is to develop a method suitable for snow-cover monitoring of forested areas. The method is based on a generalized reflectance model for snow-covered forests, which is reviewed here (Vikhamar & Solberg, 2003; Vikhamar, Solberg, & Seidel, in press). Snow-cover fraction of a pixel is estimated by constrained spectral unmixing of two Terra MODIS images (4 May 2000 and 7 May 2001) covering a forested area in southern Norway. A map with land-cover fractions, derived from a Landsat Enhanced Thematic Mapper Plus (ETM+) image, is used during the spectral unmixing to identify each pixel's endmembers (term used in spectral mixing modelling literature, referring to the "pure" spectral classes in a pixel), and to set area constraints on the forest endmembers of the pixel. ETM+ images, acquired on the same days as the MODIS images, serve to validate the estimated snow-cover fractions. Results are

presented thematically for non-forested areas, deciduous forests, coniferous forests and mixed forests of both full and patchy snow-covered situations.

2. A method for mapping the snow cover in forests (*SnowFrac*)

First, the generalized reflectance model for forests (generalized *SnowFor*) is reviewed. Secondly, it is described how the snow-cover fraction within a pixel is estimated using constrained linear spectral unmixing and a land-cover fraction map (Fig. 1). This procedure is referred to as the *SnowFrac* method.

2.1. A generalized reflectance model

Reflectance modelling is helpful to improve the understanding of the satellite-measured radiance from snow-covered forests. Therefore, a linear spectral mixture model (*SnowFor*) for snow, individual tree species (birch, pine and spruce) and snow-free ground as well as three physically based submodels to *SnowFor* (*BirchMod*, *ShadMod* and *DiffusMod*) are developed in earlier work (Vikhamar & Solberg, 2003). *BirchMod* estimates the transparency of leafless birch trees based on the density of branches. This is to account for the spectral contribution of snow/ground below individual birch trees. As opposed to leafless birch, tree crowns of spruce and pine are assumed opaque. *ShadMod* accounts for cast shadows on the snow surface caused by single trees on flat terrain. Different approaches are developed for spruce/pine and leafless birch. *DiffusMod* models shielding of the viewable sky hemisphere caused by tree crowns, as seen from the snow surface. This is to account for reduced diffuse irradiance onto the snow surface, as a consequence of the reduced viewable sky hemisphere. Generally, these submodels are based on modelling single trees within a pixel, and therefore need information about individual trees (species, height, location) and the tree density. For practical applications (snow-cover monitoring), this kind of data set is generally not available, and therefore a generalized linear spectral mixture model for snow-covered forests (referred to as generalized *SnowFor*), which uses appropriate available data as model input, is needed. The generalized *SnowFor* is derived by scaling up the model from single-tree scale to forest scale. Based on the experiences from the earlier work generalizations are made by keeping important factors, and excluding less important factors, with respect to spectral influence on the satellite-measured radiance. The generalized *SnowFor* model is described as:

$$\hat{R} = A_C R_C + A_{BR} R_{BR} + A_{SW} R_{SW} + A_{BG} R_{BG}, \quad (1)$$

where \hat{R} is the modelled pixel reflectance for a given wavelength λ and $A_C + A_{BR} + A_{SW} + A_{BG} = 1$.

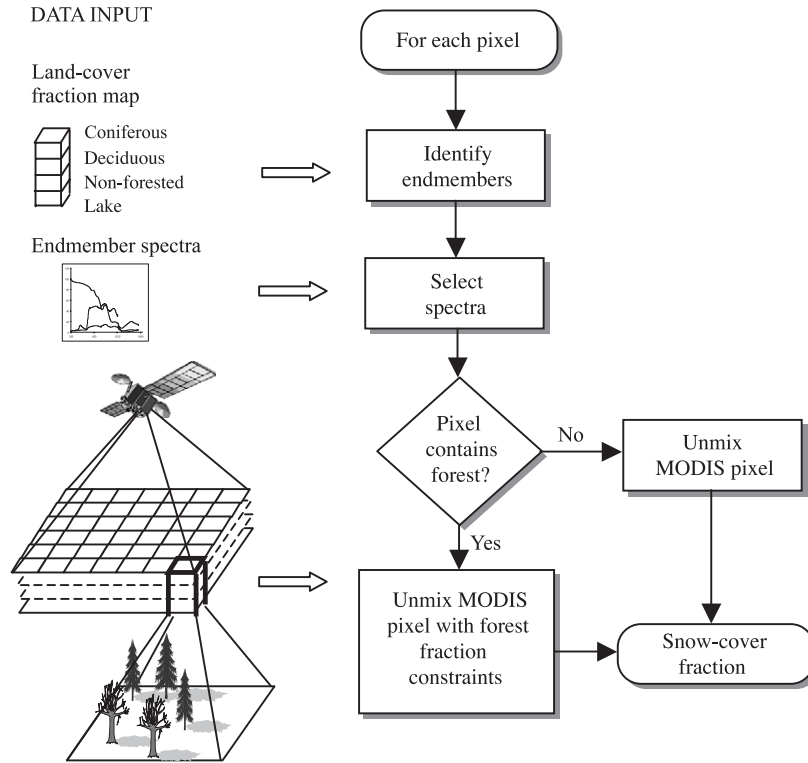


Fig. 1. Flowchart for the *SnowFrac* method, showing input data and algorithm for estimating snow-cover fraction. The land-cover fraction map is used for selection of spectra for each pixel, as well as setting constraints on the area fractions of conifer and deciduous trees.

The subscripts C and BR refer to conifer and branches of leafless deciduous trees, respectively, while the subscripts SW and BG refer to snow and bare ground, respectively. To observe consistency, the same notation is used as in the earlier work (Vikhamar & Solberg, 2003; Vikhamar et al., in press).

The generalizations are summarized as follows:

1. A single component describes conifer, since spruce and pine are rather similar in both the shape of their spectra and the natural reflectance variabilities. These observations were seen in spectra of pine and spruce tree crowns measured in the field (Fig. 7 in Vikhamar & Solberg, 2003).
2. A single component for branches describes any leafless deciduous tree species.
3. To reduce the amount of necessary input data, forest characteristics are represented by average values rather than information about individual trees within pixels. *BirchMod*, which models the leafless branch fraction, is kept for the generation of a map with land-cover fractions. The leafless branch fraction is derived by projecting branches of trees vertically on the ground using an empirical model with average tree height as input data (Fig. 2).
4. Effects of diffuse radiation for the snow surface (cast shadows from trees, shielding of the sky hemisphere by trees) are treated by the snow spectrum through the use of

multiple spectra for snow instead of explicit modelling of individual effects. Hence, both the *ShadMod* and the *DiffusMod* submodels are excluded due to their need for single-tree information as model input.

5. Effects of diffuse radiation for the conifer tree crowns are accounted for by using training areas with dense coniferous forest to determine the conifer spectrum.
6. Radiometric terrain effects for snow are accounted for by using multiple snow spectra. Terrain effects are larger for snow than for coniferous forests (Vikhamar et al., in press). Therefore, multiple spectra are applied for the snow component, but not for the conifer component. (Vikhamar et al., in press) found strong correlations between topography and land-cover specific reflectances using 30-m resolution Landsat TM images. A preliminary test with the MODIS images covering the study area in this work showed that 500-m resolution was too coarse

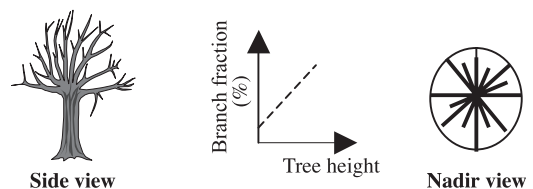


Fig. 2. *BirchMod* is applied for generating a land-cover fraction map. Branch fraction, A_{BR} , is estimated by vertically projecting leafless deciduous trees onto the ground, using tree height as input to an empirical model (Vikhamar & Solberg, 2003). Average tree height is used for the deciduous forest.

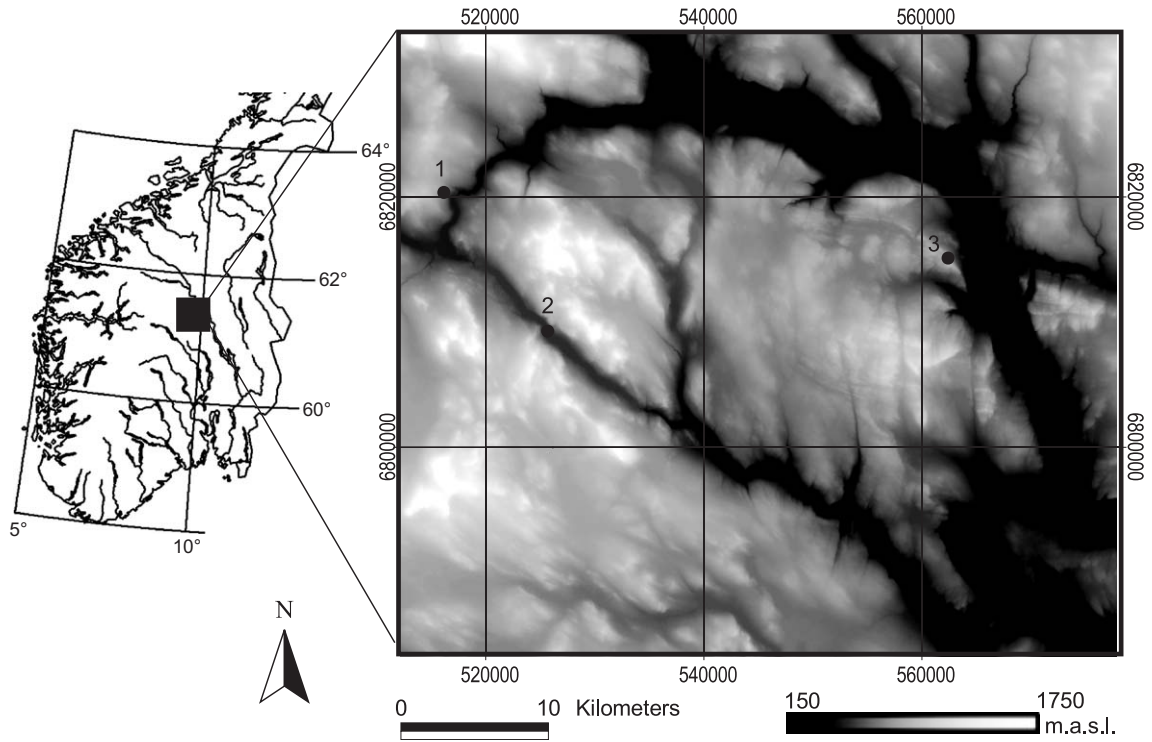


Fig. 3. Digital elevation map of the Gålå–Kvitfjell region in southern Norway (UTM coordinates). Meteorological stations are marked: (1) Skåbu (890 masl); (2) Espedalen (752 masl); and (3) Kvitfjell (1030 masl).

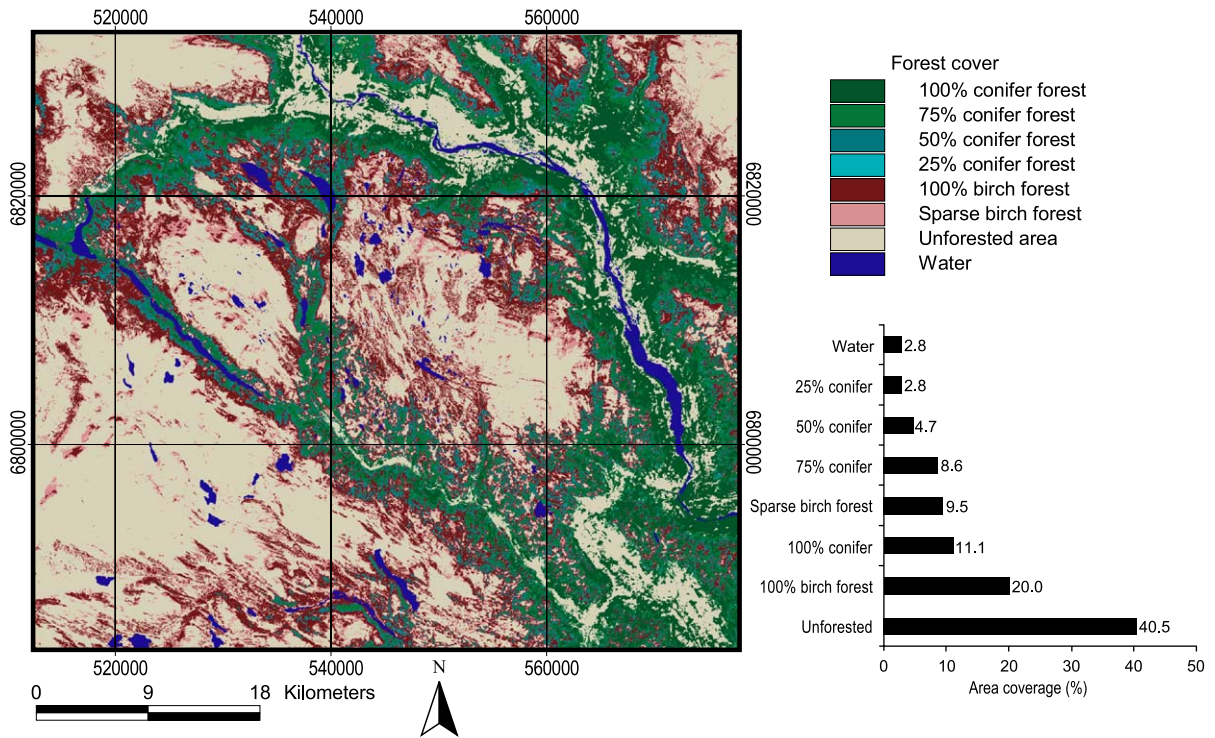


Fig. 4. Land-cover map derived from the 7 May 2001 Landsat ETM+ image (30-m resolution, UTM coordinates). The categories are rough estimates of the coverage of conifer and mountain birch. The table shows the area coverage of each category within the study area.

to find the same functional relationships by a simple illumination-terrain modelling approach. Therefore, multiple snow spectra are used instead of explicit modelling of terrain effects.

2.2. Snow-cover fraction estimation by constrained spectral unmixing

Since the generalized *SnowFor* model is a linear spectral mixture model, the snow-cover fraction of a pixel can be estimated by linear spectral unmixing of multispectral data (e.g., Adams, Smith, & Johnson, 1986). Spectral unmixing, also called mixture decomposition, has been applied for subpixel mapping of land-cover types in different environmental applications including snow-cover mapping (Nolin et al., 1993; Painter et al., 1998; Rosenthal & Dozier, 1996). The observed pixel reflectance R for a given wavelength or spectral band λ is modelled as: $R_\lambda = \hat{R}_\lambda + \varepsilon_\lambda$, where \hat{R} is the modelled pixel reflectance from a spectral mixture model (here the *SnowFor* model) and ε is the residual error, which represents the unmodelled portion of the observed reflectance. Hence, for a satellite image consisting of m spectral bands ($\lambda = 1, 2, \dots, m$), we get m equations for each pixel. This equation system can be rewritten in vector notation as:

$$r = \mathbf{E}a + \varepsilon, \tag{2}$$

where r contains the observed pixel reflectance for m spectral bands, a represents the unknown area fractions of n endmembers, \mathbf{E} is an $m \times n$ matrix representing n endmember spectra for m spectral bands and ε is the residual vector for m spectral bands. As there are more equations than unknowns ($m > n$), the equation system is overdetermined. Hence, for each pixel, the overdetermined equation system is solved for x using the least squares method to minimize the errors ε . The practice of using model constraints during the unmixing varies in the literature. Common constraints are that the endmember fractions either sum to 1 or be nonnegative and sum to not more than 1 (Rosenthal & Dozier, 1996). The first approach allows both negative area fractions and single area fractions exceeding 1, which is not physically meaningful. To give a physical sense, the area fractions must be in the interval of 0 to 1, and should also be constrained to sum to one. In this work, it is focused on benefiting from using a land-cover map, which particularly contains fractional occurrence of each the forest endmembers within a pixel. In this way, the land-cover fraction map is prior information,

Table 1
Two sets of nearly simultaneously acquired Terra MODIS (MOD02HKM) and Landsat ETM+ (177/19) images were used in the analysis

Satellite image	Date	Time (GMT)	Solar elevation
Terra MODIS	04–05–2000	11:10	44.4
Landsat ETM+	04–05–2000	10:29	43.7
Terra MODIS	07–05–2001	11:05	45.2
Landsat ETM+	07–05–2001	10:27	44.4

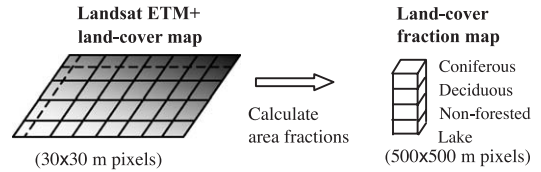


Fig. 5. A 500-m resolution land-cover fraction map was derived from the 30-m resolution Landsat ETM+ land-cover map in Fig. 4. For each pixel, the derived map contains area fractions of conifer, branches of leafless deciduous trees, non-forested area and lake.

which enable setting constraints on the forest area fractions of a pixel. The bounded variables least-squares algorithm by Stark and Parker (1995) allows setting different constraints on each of the endmember fractions, and was therefore applied for the mixture decomposition.

$$b_l \leq a \leq b_u, \tag{3}$$

b_l and b_u are the lower bounds and upper bounds of the vector a . Hence, the main idea studied here is twofold (Fig. 1). A prior generated land-cover fraction map is first used for identifying endmembers within a pixel. As a consequence, the number of endmembers, and therefore also the spectra, vary from pixel to pixel. Secondly, for pixels containing forests, the land-cover fraction map is used to set constraints on the area fractions of conifer and leafless branches during the unmixing calculation. Other area fractions are set to vary between 0 and 1. Since the algorithm of Stark and Parker (1995) does not contain a sum constraint, the area fractions are normalized based on the fraction sum. The overall aim of using a land-cover map is to reduce the number of unknown variables in the equation system, and thereby improve the estimation of the snow-cover fraction.

3. Study area and data set

A study area of 56 × 50 km surrounding the Gålå–Kvitfjell mountain region located 10 km north of Lillehammer city in southern Norway was selected for the experiments (Fig. 3). The area covers deep valleys as well as

Table 2
Overview of the constraints regarding the spectra selection and the area fractions for the spectral unmixing experiments A–F

Experiment	Land-cover map selected spectra	Forest fraction constraints	Multiple snow spectra
A	No	No	No
B	Yes	No	No
C	Yes	Yes (A_{BR}, A_C)	No
D	Yes	Yes ($A_{BR} \pm 0.1, A_C \pm 0.1$)	No
E	Yes	Yes (A_{BR}, A_C)	Yes
F	Yes	Yes ($A_{BR} \pm 0.1, A_C \pm 0.1$)	Yes

All other area fractions within a pixel vary between 0 and 1. Yes/No: description of area fraction constraint.

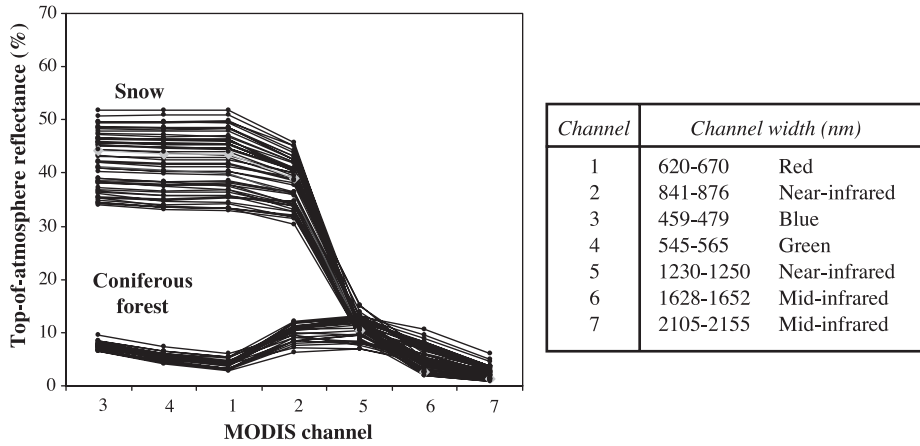


Fig. 6. MODIS spectra (4 May 2000) of snow and dense coniferous forests showing the large reflectance variability of snow as compared to coniferous forests. Average and one standard deviation snow spectra were calculated from this data set. The table describes spectral characteristics of the MODIS channels 1–7.

rounded mountain plateaus and has large variety in forest cover density (Fig. 4). The vegetation pattern is characteristic for the altitude differences in the region. Agricultural areas and rivers are located in the valley bottoms. Dense spruce forests cover the lower part of the valley sides, with a transition to sparse spruce forests mixed with mountain birch in the higher parts. On the mountain plateau, scattered mountain birch is common, while the highest areas are non-forested. Minor areas are covered with pine forests and other deciduous tree species.

Two Terra MODIS scenes (MOD02HKM: level-1b calibrated, geolocated radiances, channels 1–7, 500 × 500 m spatial resolution) were selected for the analysis (Table 1). There was full snow coverage on 7 May 2001 apart from some snow-free valleys, while on 4 May 2000, the snow coverage was thin and patchy. Both dates were characterized by melting snow. Equal weather conditions were observed on both dates at meteorological stations located in the test area (Fig. 3): no clouds, high visibility and air temperatures of 10.8 °C (4 May 2000) and 10.9 °C (7 May 2001) measured at 12 h GMT in Skåbu (890 masl), and air temperatures of 7.2 °C (4 May 2000) and 8.2 °C (7 May 2001) at 11 h GMT in Kvitfjell (1030 masl). No snow was observed in Skåbu on 4 May 2000, while 37-cm snow depth was measured on 7 May 2001. Snow-cover validation data consisted Landsat ETM+ images (30 × 30 m spatial resolution for channels 1–5, 7) acquired the same day as the MODIS images. Additionally, snow spectra and snow parameters (grain size, density, temperature, liquid water content) were measured on several locations in the study area and in Heimdalen (test site for other experiments located 30 km from the study area) during field campaigns on 6 and 7 May 2001. Spectra were measured with a portable FieldSpec spectroradiometer (350–2500 nm, 2151 channels).

Image preprocessing consisted of geometric correction and radiometric calibration. The MODIS calibrated radiance values (level 1b) were converted to top-of-atmosphere reflectance (Bruce Berriman & Rogers, 2000). The geocoding

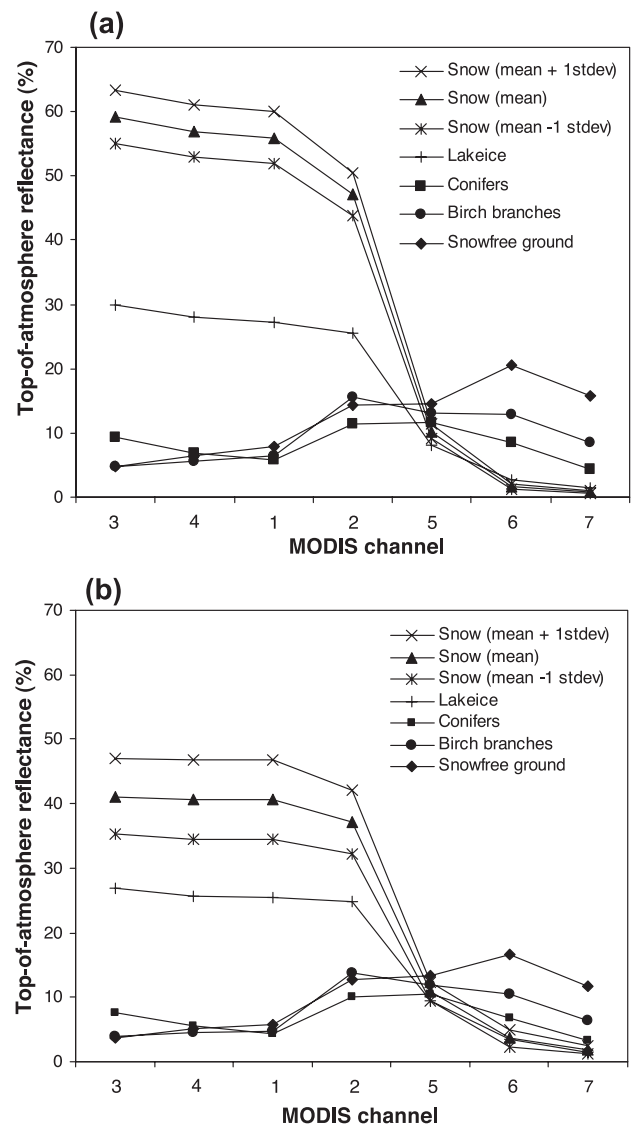


Fig. 7. Endmember spectra used in the spectral unmixing experiments: (a) 7 May 2001; and (b) 4 May 2000.

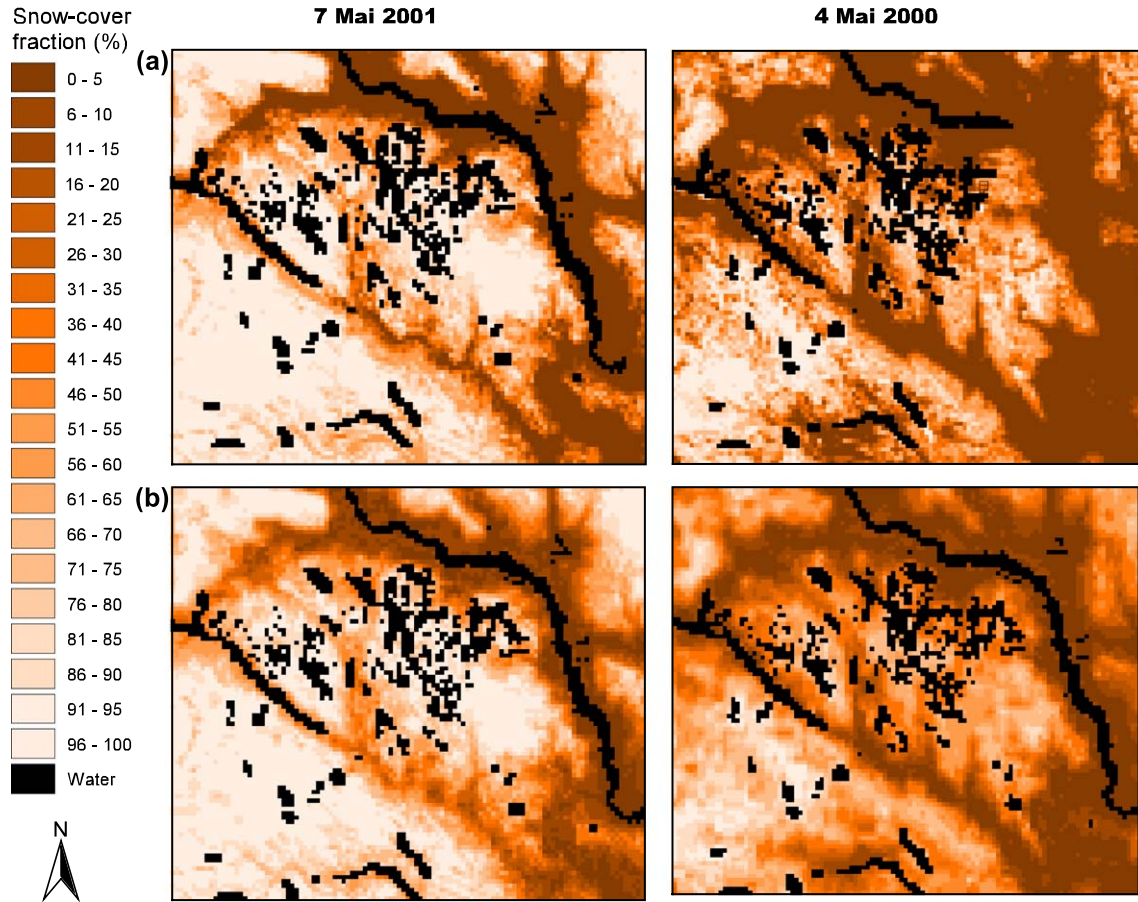


Fig. 8. The illustration shows (in percentage): (a) observed snow-cover fractions; and (b) modelled snow-cover fractions. For forested areas experiment C is presented, while for non-forested areas experiment B is shown. The snow-cover fractions do not include snow below trees. Pixels including lakes are not evaluated.

in the meta-data of the MODIS images was improved using the orthophotocorrected Landsat ETM+ images. Optimized coregistration was estimated through an iterative process consisting of: (1) resampling the ETM+ image from 30- to 500-m spatial resolution, stepwise for each 30 m in the north

and east directions; and (2) for each resampled low-resolution ETM+ image, finding the position in the MODIS image with the highest pixel-to-pixel correlation (Bernstein, Colby, Murphrey, & Snyder, 1983, p. 881). Finally, the coregistration with the overall best match was selected.

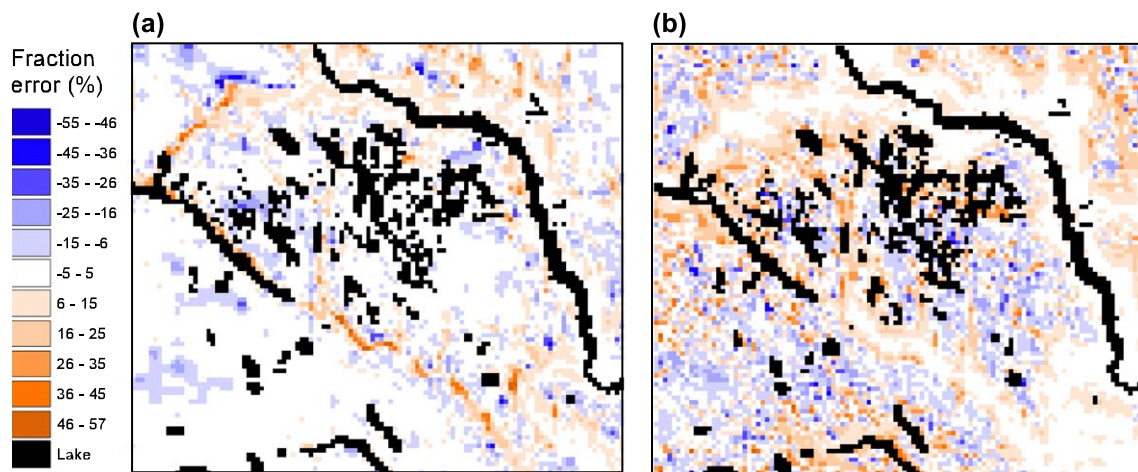


Fig. 9. Differences (fraction error) between modelled and observed snow-cover fractions from Fig. 8: (a) 7 May 2001; and (b) 4 May 2000. Red indicates model overestimation and blue is model underestimation.

A land-cover fraction map of 500-m spatial resolution was experimentally generated from the 7 May 2001 ETM+ image, because no suitable land-cover map exists for the entire study area. The map was made largely in two steps: (1) classification of 30-m spatial resolution pixels into land-cover types (Fig. 4); and (2) derivation of land-cover fractions for 500-m pixels from the 30-m resolution land-cover map, defined by the optimized coregistration position (Fig. 5). In the first step, several classification techniques (unsupervised classification, thresholding, principal components) were combined to identify appropriate land-cover types. Varying forest densities were possible to identify for 30-m resolution pixels when spruce and pine were treated as a single coniferous class. Therefore, the 30-m land-cover map contains coarse fractional classes of coniferous forest (25%, 50%, 75% and 100%). A quantification of mixtures of coniferous and deciduous forests within 30-m resolution pixels was not possible, and, therefore, the complementary part is modelled as non-forested area (bare ground). It is noteworthy that snow-covered areas with leafless mountain birch clearly separated spectrally from surrounding open snow-covered areas. For pixels that were classified as deciduous forests, the area fraction of branches was estimated by applying the *BirchMod* model (Fig. 2). A rough approximation of the average tree height ($h=3.5$ m) was applied to the empirical model $A_{BR}=0.076h+0.135$. This gives branch area fractions of 0.4 and 0.1 for pixels classified as dense and sparse deciduous forests, respectively. The 30-m land-cover map was controlled against vegetation maps (scale 1:20 000) made by the Norwegian Institute of Land Inventory, which unfortunately covered only 14% of the study area. The remaining areas were compared with lower-resolution maps containing a single forest class only.

A snow-cover fraction reference map of 500-m resolution was derived from each of the two ETM+ images by a combination of classification methods. Both supervised classification and the normalized difference snow index (NDSI) were applied on the 30-m resolution images. NDSI was applied with several user-selected thresholds, and not the thresholds proposed by Hall, Riggs, and Salomonson (1995). Furthermore, snow-cover fractions were calculated by aggregating the 30-m resolution images to 500-m resolution images using the optimized coregistration position. These snow reference maps of 500-m resolution included the snow below the trees. Therefore, the forest cover was subtracted from the snow reference maps in order to make the maps comparable to the direct snow-cover fraction output from *SnowFrac* (A_{SW} in Eq. 1). For both dates, the subtraction was made using the land-cover fraction map.

4. Experiments

The performance of the *SnowFrac* method (Fig. 1) is investigated by stepwise introducing constraints to the spec-

tral unmixing of the two MODIS images. In total, six experiments, A–F, were carried out (Table 2).

Experiment A represents regular linear spectral unmixing using the predefined selection of spectra for all pixels. In this study, spectra of snow, ice-covered lake, conifer, birch branches and snow-free ground are applied. In experiments B, C, D, E and F, the land-cover fraction map is used to identify and select endmember spectra for each pixel. Additional constraints are set on the area fractions of conifer and leafless branches in experiments C, D, E and F. For C and E, the forest area fractions are set equal to those in the land-cover fraction map, while D and F allow flexibility by letting the forest area fractions deviate by ± 0.1 .

Multiple spectra for snow are introduced in experiments E and F. Three different snow spectra are determined from estimating the average and the standard deviation of pure snow pixels observed in the two MODIS scenes. The motivation for using multiple snow spectra is to account

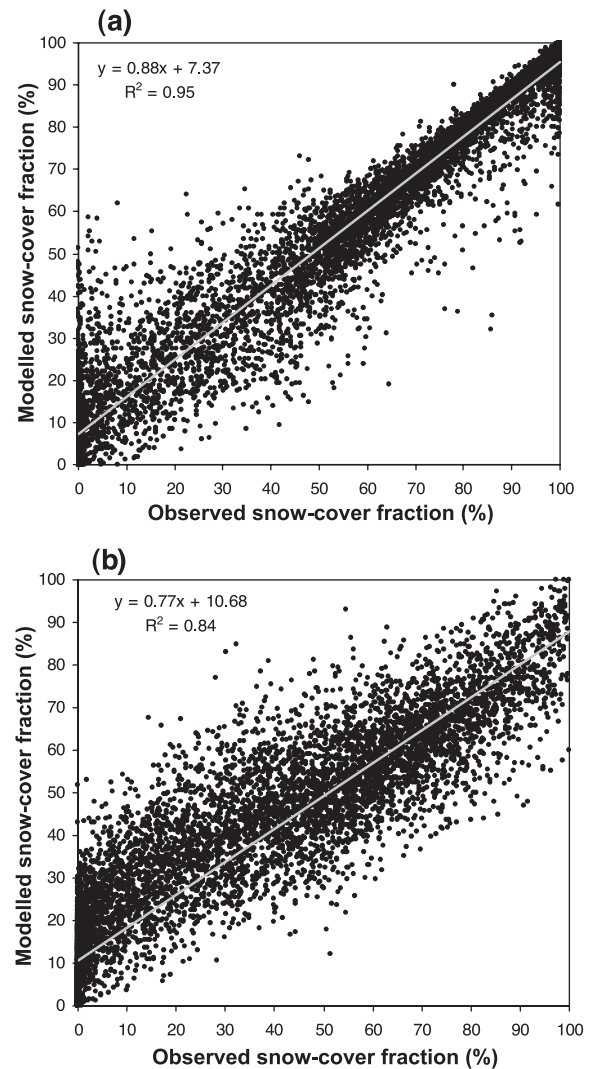


Fig. 10. Observed and modelled snow-cover fraction (experiment C), in percentage, for all forest pixels in the test area: (a) 7 May 2001; and (b) 4 May 2000. Linear regression models are displayed.

for the large reflectance variability observed for snow within a scene (Fig. 6). This variability is caused by spatial variability in physical snow properties (grain size, liquid water content), shadow effects, reflectance anisotropy and impurities on the snow surface. Using average and standard deviation of observed MODIS spectra accounts for these factors in an integrated way (see Section 2.1). The three snow spectra were evaluated for each pixel from calculating the root-mean-square (rms) of the errors ϵ . The unmixing

result with the lowest rms error for a pixel was selected as the output snow-cover fraction.

All endmember spectra used in the experiments are shown in Fig. 7. Top-of-atmosphere reflectance spectra for snow, conifer and ice-covered lake were derived from the MODIS data. Spectra of birch branches and snow-free ground were measured in situ, and calibrated to top-of-atmosphere reflectance based on the ratio of surface reflectance of snow (in situ) and top-of-atmosphere reflectance for

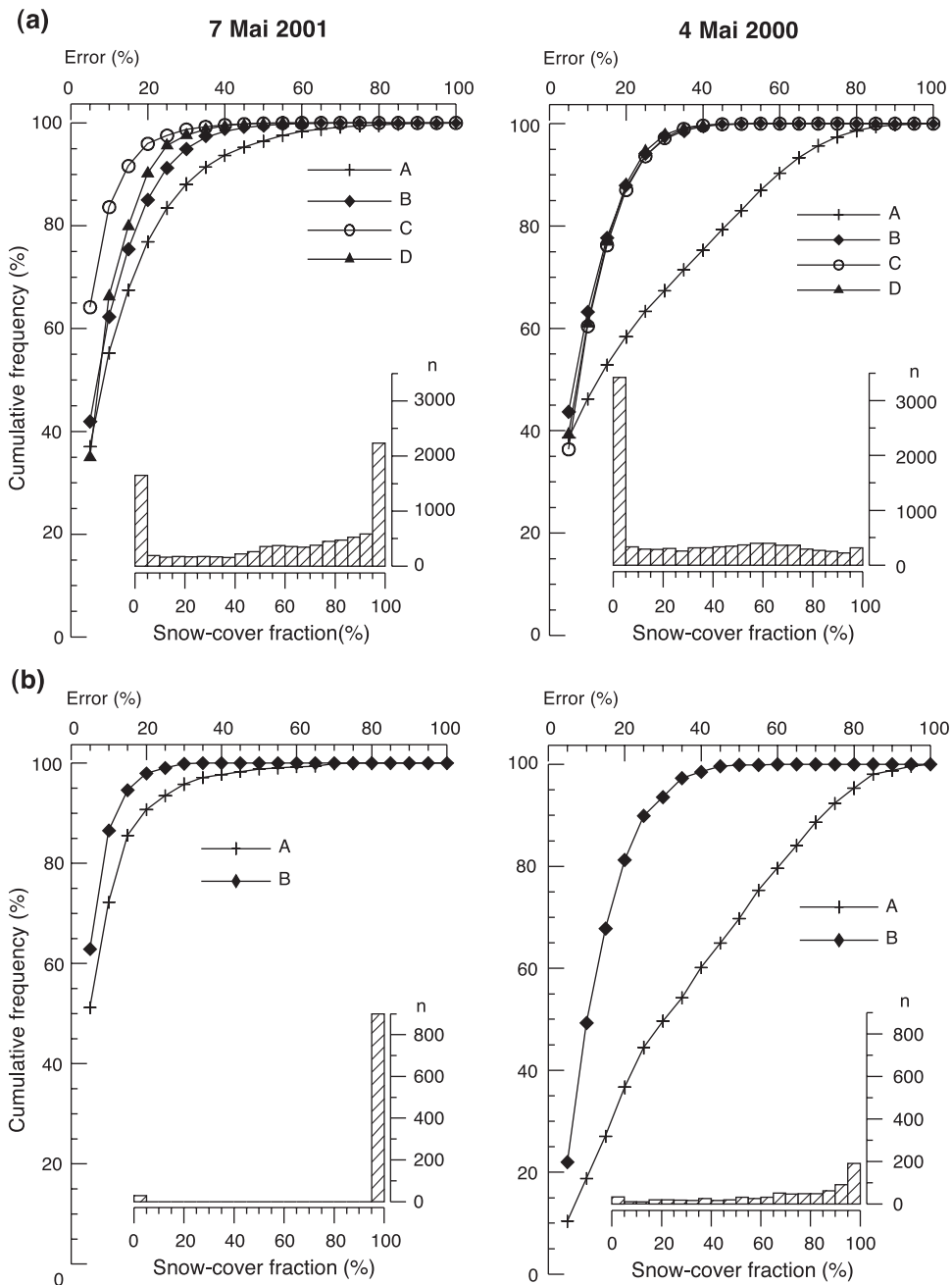


Fig. 11. Cumulative line histograms of the error differences (the absolute value of modelled observed snow-cover fraction, in percentage) for experiments A, B, C and D for 7 May 2001 (diagrams to the left) and 4 May 2000 (diagrams to the right). Experiments E and F are omitted due to large degree of overlap with experiments C and D. The diagrams are presented for pixels containing: (a) all land-cover types, except lakes; and (b) non-forested areas. Each diagram contains a column histogram (n = number of pixels) of observed snow-cover fractions.

MODIS snow pixels. Since it is not the intention of this study to focus on snow-free bare ground, these areas are handled in a simple way by generating a single ground spectrum as an average spectrum of grass and soil spectra.

5. Snow-cover mapping results

This section presents the results obtained with the *Snow-Frac* method for the Gålå–Kvitfjell study area in southern Norway. The modelled snow-cover fractions are compared with the Landsat ETM+ derived snow-cover fractions, for

both 4 May 2000 and 7 May 2001. Maps with modelled snow-cover fractions are presented in Fig. 8, showing the same main visual features as the reference maps. Pixels containing lakes were not evaluated since water-, snow- or ice-covered lakes are not yet taken into account by the model. All other forested and non-forested areas are included in experiments A and B, while experiments C, D, E and F solely treat the forested areas. Quantitative evaluation of the modelling results are presented as: (1) fraction error maps, calculated as the difference between modelled and observed snow-cover fraction (Fig. 9); (2) scatter plots of modelled versus reference snow-cover fractions (Fig. 10); (3) cumu-

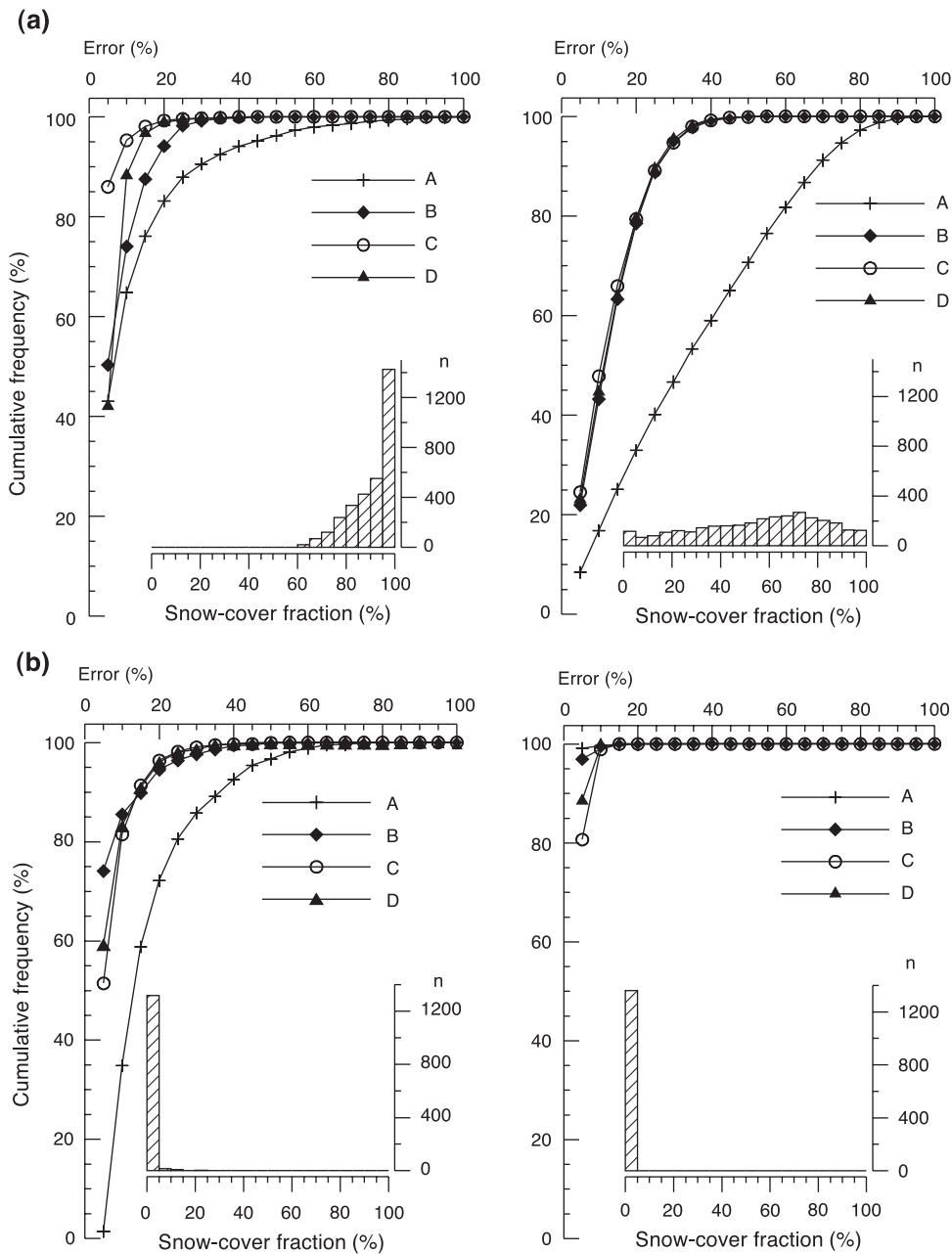


Fig. 12. The same as in Fig. 11 but for pixels containing: (a) deciduous forests; and (b) coniferous forests. The diagrams to the left represent 7 May 2001 and the diagrams to the right represent 4 May 2000.

lated histograms of the modelled fraction errors (absolute value), presented as percentage of the pixels classified with certain errors (Figs. 11, 12 and 13); and (4) aggregated snow-cover area (km²) within the study area (Fig. 14). These statistical measures are included to show different aspects of the errors. The results are first presented for the entire study area aggregated for all land-cover types. Next, the results are presented for individual land-cover types: non-forested areas, deciduous forests, coniferous forests and mixed deciduous/coniferous forests.

5.1. Entire study area

The scatter plots of all forested areas in the study area show that *SnowFrac* (experiment C) provides good snow-cover fraction estimates for both MODIS scenes (Fig. 10). *R*² values of the regression models are 0.95 and 0.85 for 7 May 2001 and 4 May 2000, respectively. The regression models indicate that low snow-cover fractions are systematically overestimated. The overestimation is most probably caused by large snow-free areas with mixtures of endmembers, which are not captured using a single spectrum for snow-free ground. High snow-cover fractions are better modelled on 7 May 2001 than on 4 May 2000, which may be explained by differences in snow conditions. Compared to 7 May 2001, the snow extent was much smaller, the snow depth was less and the snow reflectance was lower (Fig. 7).

Cumulative histograms of the fraction errors (absolute value, in percentage) aggregated for all land-cover types are compared for experiments A, B, C, D, E and F (Fig. 11a). Inquiries among hydrologic end users in Norway have shown that the users need an accuracy of about 90%. Hence,

the users accept up to 10% errors. This is the reason why the following focuses on errors of 10% and also 20% in the analysis and in Figs. 11, 12 and 13. On 7 May 2001, less than 10% error was associated with 84% (experiments C and E), 66% (experiment D), 65% (experiment F), 62% (experiment B) and 55% (experiment A) of all the pixels. Error less than 20% was obtained for 96% (experiments C and E), 90% (experiments D and F), 85% (experiment B) and 76% (experiment A) of the pixels. Overall, experiments C and E provide the best results with the lowest errors, while experiment A gives the largest errors. Similarly, on 4 May 2000, experiment A is associated with the highest errors. However, experiments B, C, D, E, and F provide almost equal results, where 58–63% of the pixels have less than 10% error, and 87–88% of the pixels have less than 20% error.

5.2. Individual land-cover types

5.2.1. Non-forested areas

On 7 May 2001, most non-forested areas were fully snow covered, while on 4 May 2000, these areas were partly snow covered (Fig. 11b). Since no trees are present, only experiments A and B are carried out for these areas. On both dates, experiment B provides better results than experiment A. On 7 May 2001, 87% of the pixels have less than 10% error, while 98% of the pixels have less than 20% error for experiment B. On 4 May 2000, the errors for experiment B are larger, with 50% and 81% of the pixels having less than 10% and 20% error, respectively. The calculated snow coverage (km²) for non-forested areas in Fig. 14 confirms the good results of experiment B, while experiment A generally underestimates the snow coverage. Taking into

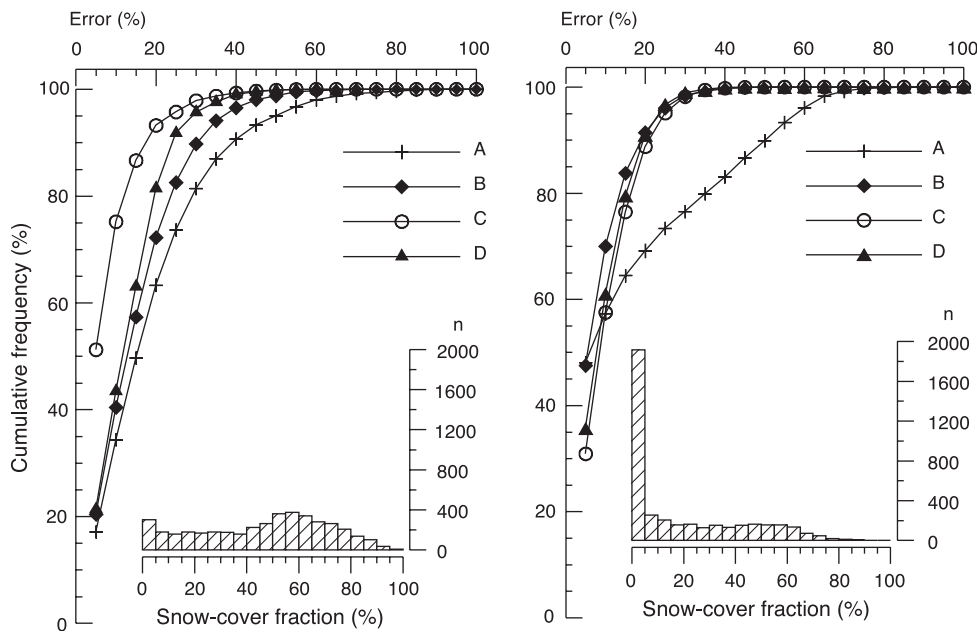


Fig. 13. The same as in Fig. 11 but for pixels containing mixed deciduous/coniferous forests. The diagram to the left represents 7 May 2001 and the diagram to the right represents 4 May 2000.

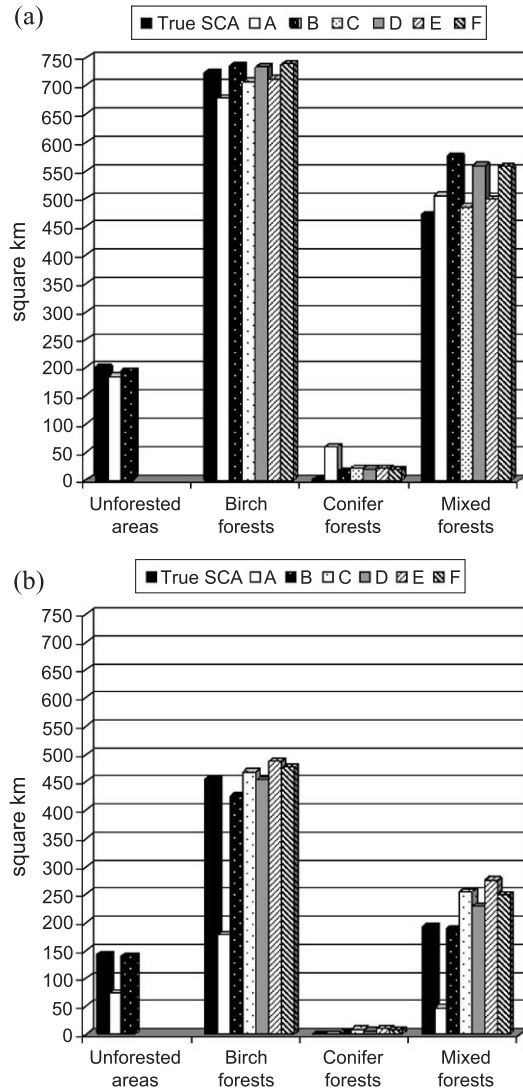


Fig. 14. Comparison of the observed and the modelled snow-covered area (km^2) for each land-cover type in the study area: (a) 7 May 2001; and (b) 4 May 2000. True SCA is the observed snow-covered area, excluding the snow below the trees. The letters A–F refer to experiments A–F.

account that only a single bare ground spectrum is applied in experiment B, these results are quite promising.

5.2.2. Deciduous forests

Full and patchy snow coverage is also validated for deciduous forests. On 7 May 2001, there was full snow coverage in 97% of the pixels containing deciduous trees, while these areas were partly snow covered on 4 May 2000 (Fig. 12a). As expected, lower errors are associated with full snow coverage than with partly snow coverage. Experiment A gives the largest errors on both dates. On 7 May 2001, experiments C and F provide the lowest errors with 95–96% of the pixels classified with less than 10% error. Additionally, experiments C, D, E and F result in 99% of the pixels classified with less than 20% error. On 4 May 2000, only 43–48% of the pixels get less than 10% error, and 78–79%

of the pixels get less than 20% error for experiments B, C, D, E and F. The aggregated snow-cover area estimates show that some under- and overestimation occurs for the experiments, except for experiment D, which correctly models the observed snow coverage (353 km^2) on 4 May 2000 (Fig. 14).

5.2.3. Coniferous forests

In the study area, most of the coniferous forests are located on the lower valley sides and in the valley bottoms. This location explains why 94% of the pixels covering coniferous forests were snow-free on 7 May 2001. Similarly, 99% of the coniferous forest pixels were snow-free on 4 May 2000. It is important to note that the coniferous forest fractions, derived from the land-cover fraction map, covered all ranges from 1% to 99%. The results are particularly good on 4 May 2000 with 98% of the pixels classified with less than 10% error for all experiments; 100% of the pixels have less than 20% error. On 7 May 2001, the errors are somewhat higher with 82–86% of the pixels classified with less than 10% errors, and 95–96% of the pixels having less than 20% errors for experiments B, C, D, E and F. Overall, the accuracy for snow-free coniferous forests is high.

5.2.4. Mixed forests

The mixed coniferous and deciduous forests constitute a transition zone between the coniferous forests on the valley sides and the birch forests on the mountain plateau. In this zone, considerably less snow is observed on 4 May 2000 than on 7 May 2001 (Fig. 13). Experiments C and E provide best results on 7 May 2001 with 75% of the pixels having less than 10% error, and 93% of the pixels having less than 20% error. On 4 May 2000, experiment B provides best results with 70% of the pixels classified with less than 10% error and 84% of the pixels classified with less than 20% error. On both dates, experiment A gives the largest errors. Most of the experiments overestimated the snow coverage in mixed forests (Fig. 14).

6. Discussion

This section discusses the classification results from experiments A–F. Perspectives for snow-cover monitoring using *SnowFrac* are also addressed.

6.1. Classification accuracy and error sources

Generally, experiments A–F show that the classification accuracy gets higher by increasing constraints in the unmixing procedure. The largest improvement occur through the use of the land-cover fraction map, which is introduced in experiment B after experiment A. The overall largest error is obtained for experiment A, which represents traditional linear spectral unmixing where the same number and types of endmember spectra are applied for all pixels in an image. Spectra judged as the most representative for the whole study

area were applied: snow, conifer, birch branches, lake ice and bare ground (Fig. 7). The results show that some of the snow-covered areas are misclassified to lake ice in pixels that do not contain ice-covered lakes. Such misclassifications are avoided in experiments B–F, because the endmember spectra are specifically selected for each pixel based on the land-cover fraction map. The use of a land-cover fraction map therefore explains the significant improvement obtained for experiments B–F, compared to experiment A.

Constraints on the forest endmember fractions represent the common difference between experiment B and experiments C–F (Table 2). Generally, on 7 May 2001, the error differences in Figs. 11, 12 and 13 show higher classification accuracy for experiments C–F than experiment B. On 4 May 2000, there are less distinct differences between experiments B–F. The snow-cover area estimates in Fig. 14 do not show these characteristics because both areas with underestimated and overestimated snow-cover fractions are included. Possible causes to the different results for the two scenes are unequal snow depth, snow area extent and physical snow properties.

Most often, experiment C provide best results, closely followed by experiment E. Generally, the use of multiple snow spectra in experiments E and F do not further improve the results of experiments C and D, respectively. The reason may be that the three snow spectra may not well enough capture the snow reflectance variability in the forested areas of the study area, since the snow spectra were derived from training areas with full snow coverage located above the tree line. Conditions may be different inside forests. In particular, accumulation of impurities on the snow surface may be larger in coniferous forests and mixed forests as compared to deciduous forests or non-forested areas (Melloh, Hardy, Davis, & Robinson, 2001). Impurities affect the snow reflectance, particularly in the visible wavelengths; an effect that was modelled by Warren and Wiscombe (1980) and recently measured by Melloh et al. (2001). Similarly, physical snow properties may have been different inside the forests than at the training areas, and variability in both liquid water content and grain size affects the snow reflectance (Dozier, 1989; Warren, 1982; Wiscombe & Warren, 1980).

There are also general error sources that concern all the experiments. The generalized *SnowFor* model, which is a linear spectral mixture model, assumes the spectral contribution to be proportional to the area extent of an endmember, and independent of its location within a pixel. Non-linear effects are likely to occur for some of the endmembers, and these effects should be investigated in the future. Currently, a linear model is used as an approximation.

For any subpixel analysis combining different image sources, the geometric coregistration of the data is crucial for the investigations. In this analysis, it was focused on obtaining high-accuracy coregistration between the MODIS and the ETM+ images. However, some geometric distortions may remain. Another general error source is related to the

assumption of equal atmospheric conditions on the two dates. This assumption is based on meteorological observations on the two dates, showing similar air temperatures, relative humidity and visibility in the study area.

6.2. Perspectives for snow-cover monitoring

Is the *SnowFrac* method suitable for operational snow-cover mapping? Monitoring makes other demands on a method as compared to a method aimed for environmental process studies. In general, a method aimed for monitoring ought to be simple, automatic and robust. Does *SnowFrac* fulfill these requirements?

The simplicity of a model is characterized by its number of variables, its need for input data as well as the availability of the input data. *SnowFrac* uses a linear mixture model, which is generalized to require a land-cover fraction map and endmember spectra in addition to the optical satellite image to be analyzed. MODIS images from the Terra and Aqua satellites are currently best suited for monitoring due to daily coverage, large number of channels and moderate spatial resolution. A spectral library may store endmember spectra of leafless branches and bare ground, while spectra for snow and conifers may be retrieved from the satellite image using selected training areas. Provided it is not already available, a land-cover fraction map may have to be generated for a new area. Primarily, *SnowFrac* is developed for local and regional snow-cover mapping. Global snow-cover mapping may be more challenging due to poor availability of global land-cover maps of high accuracy. For *SnowFrac*, the land-cover map is the key source to identify and select endmembers for a pixel.

Automatic processing is considered important when a model is run routinely on large data sets. In this work, preprocessing of the MODIS images were carried out manually to optimize the data set and the output results. However, geometric correction can be made automatically by correlation matching techniques and orbital modeling (Huseby & Solberg, 1998). Rather simple methods for atmospheric correction exist, which are based on information in the image itself without needing additional atmospheric measurements (Song, Woodcock, Seto, Lenny, & Macomber, 2001). Calibration to surface reflectance is needed when endmember spectra from a library are applied on images acquired at different times. A measure of the modelling error (root-mean-square) for a pixel is computed by the spectral unmixing algorithm. This rms error not only represents the accuracy of the snow-cover fraction estimate, but also indicates the representativity of the applied endmembers. Large rms errors may indicate less representative endmembers. The representativity of the endmembers may also be explored through an unconstrained spectral unmixing approach. Negative endmember fraction values may be an indication of missing endmembers.

The robustness of a model includes the reliability and the accuracy of the resulting output data. Presently, *SnowFrac*

has only been evaluated for two different scenes of the same study area. The results are promising, but considerably more validation is needed to evaluate the method. Therefore, a simple snow monitoring system for forests may be set up for evaluation purposes by regularly mapping a few selected test areas, where meteorological observations and in situ snow surveys are available as validation data.

The land-cover fraction map makes *SnowFrac* flexible for application. For hydrological applications, an estimate of the total snow-cover area, including the snow below trees, is required. For the energy balance in climate models, an estimate of the area extent of snow between the trees may be of higher interest than information about the snow below trees. *SnowFrac* fulfills these requirements through an assumption made for the snow below trees for the two cases (Vikhamar & Solberg, 2003): (1) full snow coverage; and (2) patchy snow coverage. When full snow coverage is observed around the tree crowns, snow is also assumed present below the trees. When snow-free areas are observed between trees, completely snow-free areas are assumed below the trees. A simple criterion may be introduced to judge whether the areas below the trees should be included in the final modelled snow-cover fraction of a pixel. This criterion consists of summarizing the snow-cover fraction resulting from the unmixing procedure and the forest fractions for a pixel ($A_{SW} + A_C + A_{BR}$). If the sum equals 1, full snow coverage is assumed, and, thus, the total pixel area is counted as snow covered. If the sum is less than 1, patchy snow coverage is assumed and A_{SW} is the resulting snow-cover fraction. This shows an additional advantage of applying a land-cover fraction map in the snow-cover mapping algorithm.

7. Conclusions and future work

In this article, a method for mapping the snow cover in forests is presented (*SnowFrac*). The method uses a linear spectral mixture model including endmembers for snow, conifer, branches of leafless deciduous trees and snow-free ground. *SnowFrac* estimates the snow-cover fraction of a pixel by spectral unmixing and endmember constraints. A land-cover fraction map is applied in the unmixing process to: (1) identify the number and types of endmembers for a pixel; and (2) set constraints on the area fractions of the forest endmembers. This reduces the number of unknowns in the equation system and should thereby improve the resulting snow-cover fraction estimate.

SnowFrac was tested on Terra MODIS images (500×500 m spatial resolution, channels 1–7) from 4 May 2000 and 7 May 2001 of the Gålå–Kvitfjell study area in southern Norway. Snow-cover fractions were estimated from the MODIS images and compared with Landsat ETM+ derived snow-cover fractions. Six experiments were carried out (Table 2), each with different endmember constraints (no endmember constraints, land-cover map selected end-

members, forest fraction constraints and multiple snow spectra).

The results demonstrate that the snow-cover fraction estimates are enhanced by increasing constraints introduced to the unmixing procedure. Largest improvement occurs when endmembers are selected for each pixel based on the land-cover fraction map. The classification accuracy including both forested and non-forested areas shows that 96% of the pixels are classified with less than 20% error (absolute units) on 7 May 2001. The corresponding figure for 4 May 2000 is 88% of the pixels. For the forested areas, linear regression models of observed and modelled snow-cover fractions result in R^2 values of 0.95 and 0.85 for 7 May 2001 and 4 May 2000, respectively. Largest errors are obtained for the experiment representing traditional linear spectral unmixing using the same number and types of endmember spectra for all pixels.

The results of this study are quite encouraging for further developing *SnowFrac*. Therefore, more evaluations should be carried out, as well as quantitative comparisons with other snow-cover mapping methods. *SnowFrac* fulfills some of the requirements for a mapping method aimed for monitoring. Further research should focus on enhanced modelling of snow-free ground. One approach is to improve the land-cover fraction map by including appropriate spectral ground classes for each pixel, and combine with a library of endmember spectra describing the temporal evolution of each class.

Acknowledgements

The authors thank their colleagues and friends for their assistance during fieldwork and valuable suggestions to the manuscript. This research was financed by the Department of Geosciences, University of Oslo, Norway, and the Norwegian Computing Center, Norway.

References

- Adams, J. B., Smith, M. O., & Johnson, P. E. (1986). Spectral mixture modeling: a new analysis of rock and soil types at the Viking Lander 1 site. *Journal of Geophysical Research*, *91*(8), 8098–8112.
- Barnett, T. P., Dümenil, L., Schlese, U., Roeckner, E. R., & Latif, M. (1989). The effect of Eurasian snowcover on regional and global climate variations. *Journal of the Atmospheric Sciences*, *46*(5), 661–686.
- Baumgartner, M. F., & Rango, A. (1995). A microcomputer-based alpine snow-cover analysis system (ASCAS). *Photogrammetric Engineering and Remote Sensing*, *61*(12), 1475–1486.
- Beniston, M. (1997). Variations of snow depth and duration in the Swiss Alps over the last 50 years: Links to changes in large-scale climatic forcings. *Climatic Change*, *36*, 281–300.
- Bernstein, R., Colby, C., Murphrey, S. W., & Snyder, J. P. (1983). Image geometry and rectification. In D. S. Simonett, F. T. Ulaby (Eds.), *Manual of remote sensing: theory, instruments and techniques, vol. 1* (2nd. ed.) (pp. 873–920). American Society of Photogrammetry, The Sheridan Press.
- Bruce Berriman, G., & Rogers, J. (2000). *MODIS Level 1B product user's guide*. MD, USA: NASA/Goddard Space Flight Center (MCST document).

- Cess, R. D., Potter, G. L., Zhang, M. H., Blanchet, J. P., Chalisa, S., Colman, R., Dazlich, D. A., Del Genio, A. D., Dymnikov, V., Galin, V., Jerrett, D., Keup, E., Lacis, A. A., Le Treut, H., Liang, X. Z., Mahfouf, J. F., McAvaney, B. J., Meleshko, V. P., Mitchell, J. F. B., Morcrette, J. J., Norris, P. M., Randall, D. A., Rikus, L., Roeckner, E., Royer, J. F., Schlese, U., Sheinin, D. A., Slingo, J. M., Sokolov, A. P., Taylor, K. E., Washington, W. M., Wetherald, R. T., & Yagai, I. (1991). Interpretation of snow-climate feedback as produced by 17 general circulation models. *Science*, 253, 888–892.
- Cohen, J., & Entekhabi, D. (2001). The influence of snow cover on Northern Hemisphere climate variability. *Atmosphere–Ocean*, 39(1), 35–53.
- Dozier, J. (1989). Spectral signature of alpine snow cover from the Landsat Thematic Mapper. *Remote Sensing of Environment*, 28, 9–22.
- Gjærevoll, O. (1956). The plant communities of the Scandinavian alpine snow-beds. *Det Kongelige Norske Videnskabers Selskabs Skrifter*, 1, 1–405.
- Haefner, H., Seidel, K., & Ehrler, C. (1997). Applications of snow cover mapping in high mountain regions. *Physics and Chemistry of the Earth*, 22(3–4), 275–278.
- Hall, D. K., Foster, J. L., Salomonson, V. V., Klein, A. G., & Chien, J. Y. L. (2001). Development of a technique to assess snow-cover mapping errors from space. *IEEE Transactions on Geoscience and Remote Sensing*, 39(2), 432–438.
- Hall, D. K., Kelly, R. E. J., Riggs, G. A., Chang, A. T. C., & Foster, J. L. (2002). Assessment of the relative accuracy of hemispheric-scale snow-cover maps. *Annals of Glaciology*, 34, 24–30.
- Hall, D. K., Riggs, G. A., & Salomonson, V. V. (1995). Development of methods for mapping global snow cover using Moderate Resolution Imaging Spectroradiometer data. *Remote Sensing of Environment*, 54(2), 127–140.
- Huseby, R. B., & Solberg, R., 1998. A model-based approach for geometric correction of optical satellite images. NR Report No. 932, Norwegian Computing Center, Oslo, Norway.
- Jones, H. G. (1999). The ecology of snow-covered systems: A brief overview of nutrient cycling and life in the cold. *Hydrological Processes*, 13, 2135–2147.
- Klein, A. G., Hall, D. K., & Riggs, G. A. (1998). Improving snow cover mapping in forests through the use of a canopy reflectance model. *Hydrological Processes*, 12(10–11), 1723–1744.
- König, M., Winther, J. G., & Isaksson, E. (2001). Measuring snow and glacier ice properties from satellite. *Reviews of Geophysics*, 39(1), 1–27.
- Lundquist, D., Lunde, A. E., & Bøe, P. C. (1996). The 1995 flood in the Glomma and Lågen river basins. Technical report, Glommens og Laagens brukseierforening, Oslo, Norway.
- Marks, D., Kimball, J., Tingey, D., & Link, T. (1998). The sensitivity of snowmelt processes to climate conditions and forest cover during rain-on-snow: A case study of the 1996 Pacific Northwest flood. *Hydrological Processes*, 12(10–11), 1569–1587.
- Melloh, R. A., Hardy, J. P., Davis, R. E., & Robinson, P. B. (2001). Spectral albedo/reflectance of littered forest snow during the melt season. *Hydrological Processes*, 15, 3409–3422.
- Metsämäki, S., Vepsäläinen, J., Pulliainen, J., & Sucksdorff, Y. (2002). Improved linear interpolation method for the estimation of snow-covered area from optical data. *Remote Sensing of Environment*, 82, 64–78.
- Nolin, A. W., Dozier, J., & Mertes, L. A. K. (1993). Mapping alpine snow using a spectral mixture modeling technique. *Annals of Glaciology*, 17, 121–124.
- Painter, T. H., Roberts, D. A., Green, R., & Dozier, J. (1998). The effect of grain size on spectral mixture analysis of snow-covered area from AVIRIS data. *Remote Sensing of Environment*, 65, 320–332.
- Roesch, A., Wild, M., Gilgen, H., & Ohmura, A. (2001). A new snow cover fraction parametrization for the ECHAM4 GCM. *Climate Dynamics*, 17(12), 933–946.
- Romanov, P., Gutman, G., & Csiszar, I. (2000). Automated monitoring of snow cover over North America with multispectral satellite data. *Journal of Applied Meteorology*, 39, 1866–1880.
- Rosenthal, W., & Dozier, J. (1996). Automated mapping of montane snow cover at subpixel resolution from the Landsat Thematic Mapper. *Water Resources Research*, 32(1), 115–130.
- Solberg, R., & Andersen, T. (1994). An automatic system for operational snow-cover monitoring in the Norwegian mountain regions. *Proceedings of IGARSS 1994 symposium* (pp. 2084–2086). Pasadena, CA, USA: IEEE.
- Solberg, R., Hiltbrunner, D., Koskinen, J., Guneriusson, T., Rautiainen, K., & Hallikainen, M. (1997). Snow algorithms and products—review and recommendations for research and development. NR Report No. 924, Norwegian Computing Center, Oslo, Norway.
- Song, C., Woodcock, C. E., Seto, K. C., Lenny, M. P., & Macomber, S. A. (2001). Classification and change detection using Landsat TM data: When and how to correct atmospheric effects? *Remote Sensing of Environment*, 75, 230–244.
- Sorteberg, H. K., Engeset, R. V., & Udnæs, H. C. (2001). A national network for snow monitoring in Norway: Snow pillow verification using observations and models. *Physics and Chemistry of the Earth, Part C: Solar–Terrestrial and Planetary Science*, 26(10–12), 723–729.
- Stark, P. B., & Parker, R. L. (1995). Bounded-variable least-squares: An algorithm and applications. *Computational Statistics*, 10, 129–141.
- Sui, J., & Koehler, G. (2001). Rain-on-snow induced flood events in Southern Germany. *Journal of Hydrology*, 252, 205–220.
- Vikhamar, D., & Solberg, R. (2003). Subpixel mapping of snow cover in forests by optical remote sensing. *Remote Sensing of Environment*, 84(1), 69–82.
- Vikhamar, D., Solberg, R., & Seidel, K. (2003). Reflectance modelling of snow-covered forests in hilly terrain. *Photogrammetric Engineering and Remote Sensing*, in press.
- Walker, D. A., Halfpenny, J. C., Walker, M. D., & Wessman, C. (1993). Long-term studies of snow–vegetation interactions. *BioScience*, 43, 281–301.
- Warren, S. G. (1982). Optical properties of snow. *Reviews of Geophysics and Space Physics*, 20(1), 67–89.
- Warren, S. G., & Wiscombe, W. J. (1980). A model for the spectral albedo of snow: II. Snow containing atmospheric aerosols. *Journal of Atmospheric Sciences*, 37, 2734–2745.
- Winther, J. G., & Hall, D. K. (1999). Satellite-derived snow coverage related to hydropower production in Norway: Present and future. *International Journal of Remote Sensing*, 20(15–16), 2991–3008.
- Wiscombe, W. J., & Warren, S. G. (1980). A model for the spectral albedo of snow: I. Pure snow. *Journal of Atmospheric Sciences*, 37, 2712–2733.
- Wold, K. (1992). *Water, snow and ice, volume 3 of National Atlas of Norway*. Norwegian Mapping Authority, in Norwegian.